# Joint Estimation of Ice Sheet Vertical Velocity and Englacial Layer Geometry from Multipass Synthetic Aperture Radar Data

1st Gordon Ariho
Center for Remote Sensing and
Integrated Systems (CReSIS)
University of Kansas
Lawrence, KS USA
gariho@ku.edu

2<sup>nd</sup> John D. Paden
Center for Remote Sensing and
Integrated Systems (CReSIS)
University of Kansas
Lawrence KS, USA
paden@ku.edu

3<sup>rd</sup> Andrew Hoffman

Dept. of Earth & Space Sciences.

University of Washington

Seattle, WA USA
hoffmaao@uw.edu

4th Knut A Christianson
Earth and Space Sciences,
Program on Climate Change,
& Quaternary Research Center
University of Washington
Seattle, WA USA
knut@uw.edu

5<sup>th</sup> Nicholas Holschuh Department of Geology, Amherst College Amherst, MA USA nholschuh@amherst.edu

Abstract— Ice dynamics are a major factor in sea level rise and future sea-level rise projections [1]. The vertical velocity profile of the ice is one major knowledge gap in both observations and model experiments. We propose to apply multipass differential interferometric synthetic aperture radar (DInSAR) techniques to data from the Multichannel Coherent Radar Depth Sounder (MCoRDS) to measure the vertical displacement of englacial layers. Estimation of englacial layer vertical displacement requires compensating for the spatial baseline between interferometric antenna pairs using radar trajectory information and estimates of the cross-track layer slope from direction of arrival (DOA) analysis, but airborne systems suffer from unknown spatial baseline errors. The current DInSAR algorithm assumes zero error in the array position information when inferring displacement and the direction of arrival for subsurface scatterers, which means that unincorporated baseline errors map into errors in cross-track slope and vertical velocities. Here we demonstrate a maximum likelihood estimator that jointly estimates the vertical velocity, the cross-track internal layer slope, and the unknown baseline error due to GPS and Inertial Navigation System (INS) errors.

Keywords— multipass, DInSAR, radar sounder, interferometry, tomography, radioglaciology

# I. INTRODUCTION

Radar has been extensively applied in remote sensing of ice sheets, with the generation of nadir, SAR focused imagery the dominant application of radar data. These data products are typically used to measure ice thickness and internal-layer geometry. This paper focuses on the new application of multipass radar sounder data for englacial layer tomography and interferometry. This allows us to use radar remote sensing to measure small scale changes in the ice-sheet subsurface. Direct measurements of subsurface deformation have the

potential to constrain the fluidity and basal resistance parameters that control ice flow and reduce uncertainties in predicting ice-sheet contributions to sea level rise.

Differential Interferometric Synthetic Aperture Radar (DInSAR) [2] reveals the displacement between two data acquisitions over the same spatial region (the radar profile). This introduces an additive phase term,  $\Delta\phi_d$ , that is independent of the baseline;  $\Delta\phi_d=4\pi d/\lambda$ , where d is the relative scatterer displacement projected onto the slant range direction. The flattened interferometric phase,  $\phi_{int}$ , now comprises both the altitude and motion contributions respectively. In the case of ice sheet internal layers, vertical displacement is estimated by measuring the interferometric phase, and compensating for the spatial baseline using precise trajectory information and estimates of the cross-track layer slope from direction of arrival (DOA) analysis:

$$\phi_{int} = -\frac{4\pi}{\lambda} \frac{B_{\perp} z}{R \sin \theta_i} + \frac{4\pi}{\lambda} d, \qquad (1)$$

where  $\lambda$  is the wavelength, R is the slant range to the target,  $\theta_i$  is the DOA (layer slope),  $B_{\perp}$  is the perpendicular component of the baseline between passes, and z is the altitude from the reference plane.

With knowledge of the radar position during both the baseline and monitor radar acquisition, DInSAR's accuracy is on the order of a small fraction of the wavelength in monitoring ground displacement along the radar line of sight (LOS). But unlike ground-based Autonomous phase-sensitive Radio-Echo Sounders (ApRES) that can be precisely positioned, airborne systems suffer from unknown baseline errors. Direction of arrival (DOA) estimation, a necessary input to the traditional DInSAR algorithm, assumes the position information is

accurate, an assumption that is violated by most airborne data positioned using Global Positioning System (GPS) and Inertial Navigation System (INS) data. We propose to improve the DInSAR algorithm for use in multipass radar sounding of ice sheets by implementing a maximum likelihood estimator that jointly estimates the vertical displacement, the cross-track internal layer slope, and the unknown baseline error due to GPS and Inertial Navigation System (INS) errors.

# II. METHODOLOGY

# A. Wideband Signal Model

To formulate the wideband signal model, we decompose the wideband signals into several narrowband signals using a filter bank. The received signal is a superposition of signals from multiple sources that are received by the sensor array simultaneously. For Q sources, if we consider a narrowband component with a center frequency  $\omega_k$  at snapshot index m, we can write the received signal as:

$$\mathbf{x}(m,\omega_k) = \mathbf{A}(\omega_k)\mathbf{s}(m,\omega_k) + \mathbf{n}(m,\omega_k),$$

where m = 1, ..., M and k = 1, ..., K; A is the steering matrix, s is the source signal, and n is the additive noise. Since the steering vectors of A don't depend on m, we write a single matrix expression for all snapshots as:

$$X(\omega_k) = A(\omega_k)S(\omega_k) + N(\omega_k), \tag{3}$$

where **X** is  $P \times M$ , **A** is  $P \times Q$ , **S** is  $Q \times M$ , **N** is  $P \times M$ , and Q < P.

### B. Maximum Likelihood Estimator (MLE)

DOA estimation using MLE maximizes the likelihood that the received signal came from a particular angle  $(\theta)$ . By assuming that the noise  $\boldsymbol{n}$  is a stationary, ergodic, and Gaussian process of zero mean and variance  $\sigma^2 \boldsymbol{I}$  with statistically independent samples, we can write the joint density function of the sampled data as:

$$f(\mathbf{X}) = \prod_{m=1}^{M} \frac{1}{\pi \det[\sigma^2 \mathbf{I}]} \exp\left(-\frac{1}{\sigma^2} |\mathbf{x}(m, \omega_k) - \mathbf{A}(\theta) \mathbf{s}(m, \omega_k)|^2\right). \tag{4}$$

The log likelihood function is given by:

$$L(\theta) = -MP \log \sigma^2 - \frac{1}{\sigma^2} \sum_{m=1}^{M} |x(m, \omega_k) - A(\theta)s(m, \omega_k)|^2,$$
(5)

where the constant terms have been disregarded. We can further write the log-likelihood function as:

$$L(\theta) = \sum_{m=1}^{M} |P_{A(\theta)}x(m,\omega_k)|^2 = \text{Tr}(P_{A(\theta)}R),$$
(6)

where  $P_{A(\theta)} = A(\theta) (A^H(\theta)A(\theta))^{-1} A^H(\theta)$  is the projection of the steering matrix and Tr() is the trace operator. For deterministic MLE, the maximum likelihood estimate is done by maximizing the deterministic cost function below, assuming that the noise variance and target signal are unknown but non-random [3]:

$$J_{MLE} = \text{Tr}(\boldsymbol{P}_{\boldsymbol{A}(\theta)}\boldsymbol{R}). \tag{7}$$

MLE seeks to maximize the cost function,  $J_{MLE}$  such that:

$$\theta = \arg\max_{\theta} (J_{MLE}). \tag{8}$$

# C. Wideband Maximum Likelihood Estimator (WMLE)

Wideband MLE is realized by subdividing the signal bandwidth into K sub-bands and the narrowband MLE is applied to the combined likelihood function. This is the summation of all the individual likelihood functions assuming the sub-bands are independent [4]. The wideband MLE cost function then becomes:

$$J_{WMLE} = \sum_{k=1}^{K} J_{MLE}(\omega_k), \tag{9}$$

where  $J_{MLE}(\omega_k)$  is the narrowband MLE cost function at frequency  $\omega_k$ . Wideband MLE maximizes the cost function such that:

$$\theta = \arg\max_{\theta} (J_{WMLE}). \tag{10}$$

# D. Multipass Interferometry

Multipass DInSAR techniques are applied to the MCoRDS data to measure the vertical displacement of englacial layers [5]. MCoRDS [6] is a multichannel radar, developed by the Center for Remote Sensing and Integrated Systems (CReSIS) that has up to 15 cross-track antenna elements (4 on the left wing, 7 on the fuselage, and 4 on the right wing), which are used for array processing [6]. The scattering sources for the DInSAR measurements are quasi-specular near-horizontal englacial layers throughout the ice column as shown in Fig. 1.

The phase difference between two radar passes taken at different times gives an indication of the average vertical velocity of the layer under investigation between those two passes [5].

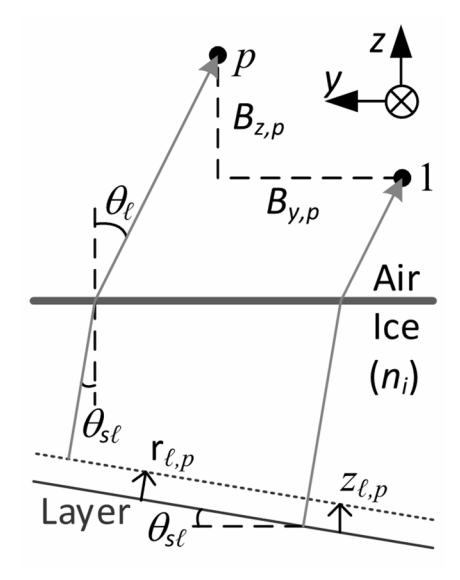


Fig. 1. Multipass geometry

If we consider a set of P passes  $(p=1,\ldots,P)$ , the crosstrack geometry shown in Fig. 1 shows that  $B_{z,p}$  and  $B_{y,p}$  are the z and y components respectively of the  $p^{th}$  baseline vector between pass 1 and the  $p^{th}$  pass.  $\theta_l$  is the Direction of Arrival (DOA) of the signal in air, and  $\theta_{sl}$  is the cross-track slope of the internal layer, l.  $\theta_{sl}$  is also equal to the DOA within the ice. Using (1), which makes use of the plane wave approximation, and subtracting the phase for pass p from that of pass 1, we get the interferometric phase,  $\phi$ , due to the spatial baseline and layer displacement for pass p relative to pass 1 as:

$$\phi = -B_{z,p}k\cos\theta_l + B_{y,p}k\sin\theta_l + r_{l,p}k,\tag{11}$$

where k is the wavenumber in air, by Snell's law  $sin \ \theta_l = n_i sin \ \theta_{sl}$  where  $n_i$  is the refraction index of ice, and  $n_{l,p}$  is the range displacement of layer, l. The layer slope is assumed to remain the same over the collection period of the passes.

We can now use classic tomographic synthetic aperture radar (SAR) techniques [7] with (11) to estimate  $\theta_l$ . We briefly present the algorithmic steps employed in DInSAR processing below (summarized in Fig. 2).

# E. DInSAR algorithm

The generalized methodology can be separated into two steps: coregistration, and estimation of interferometric phase. We first describe the processes involved in each of these steps before outlining the joint maximum likelihood estimator that unites these steps in a single framework.

# Coregistration

SAR interferometry requires pixel-to-pixel matching between common features in SAR image pairs. Thus coregistration, which aligns the SAR images from two passes, is an essential step for the accurate determination of phase difference. We refer to the reference image as the baseline image and use the term monitor images to refer to the images that we process relative to the baseline image. Coregistration of monitor SAR images from each channel of MCoRDS and from each pass is applied with a time shift to all passes based on the correlation of each monitor image with the baseline image. The imprecise repeat-pass geometry combined with cross-track gradients in layer slope complicate the process of coregistering image pairs and require corrections for positioning of antenna elements (motion compensation) and the direction of arrival of englacial reflectors. These corrections represent the primary differences in airborne DInSAR compared to previous groundbased englacial interferometry methodologies.

# Motion compensation

After along-track resampling to interpolate data to a common radar coordinate system, a time-delay is applied in the frequency-domain to the monitor images to compensate for the differences in elevation between flights. The monitor and baseline images are then later flattened relative to the surface using GPS baseline corrections.

# Estimation of direction of arrival

Cross-track slope compensation applies a phase correction after motion compensation and before array processing based on the estimated cross-track slope using (11).

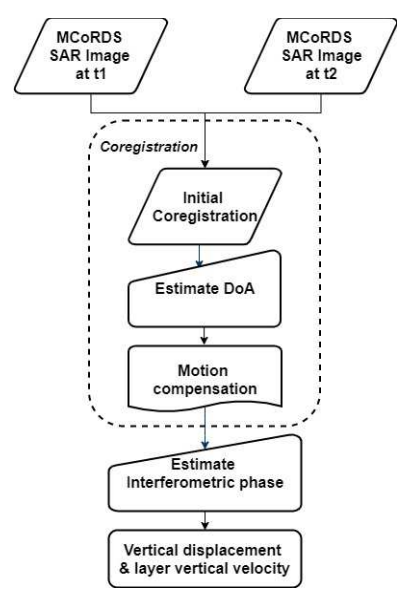


Fig. 2. DInSAR Algorithm

The slopes are calculated using the Multiple Signal Classification (MUSIC) array processing method to estimate the DOA of the returned signal, which can be related to the reflector geometry and the mean slope of reflectors over a specified range bin using Snell's law.

Interferometric phase difference and displacement estimation

Calculation of the interferometric phase is done by cross correlating the complex images in the frequency domain. These complex correlation coefficients record the wrapped phase differences between the monitor and baseline profiles that can be unwrapped and used (with assumptions for the density and permittivity of the ice) to calculate relative displacement of the layers. The layer displacement with precise knowledge of the timing between measurements can be used to calculate the vertical velocity of the layer.

# F. Joint estimation

The process of coregistering images and incrementally applying corrections for layer slopes and antenna element positions can be unified with an inverse framework that solves for poorly constrained parameters that control each correction iteratively (Fig. 3). This method can also formally treat uncertainty in the spatial baseline, improving the estimates for the glaciological parameters of interest. Here, we apply the maximum likelihood estimator (MLE) algorithm, which can be used to estimate parameters of an assumed probability distribution given a set of observational data. We chose this method because MLE is the most efficient estimator when the model is correctly assumed and results in unbiased estimates for large samples. This method fits the data by maximizing a log-likelihood function, which we use to introduce the implementation of the algorithm.

From (5), the log likelihood function for the joint estimation of the parameters for each SAR pixel can be written as:

$$L_{r,c} = -MP \log \sigma^2 - \frac{1}{\sigma^2} \sum_{m=1}^{M} |x_{r,c} - A(\theta_{l,r,c}, v_{l,r,c}, B_{y_c}, B_{z_c}) s_{r,c}|^2,$$
(12)

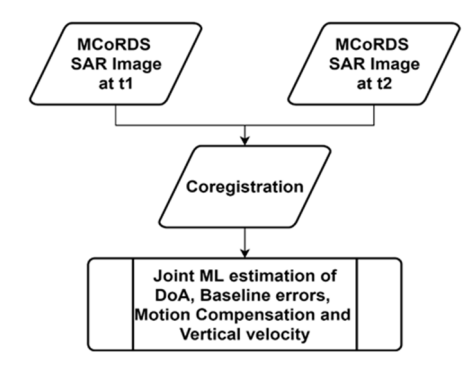


Fig. 3. Joint estimation framework

where the subscript r and c represent range bin (rows) and range line (column) indices respectively,  $B_{y_c}$  and  $B_{z_c}$  are baseline errors,  $v_{l,r,c}$  is the vertical velocity, and  $\theta_{l,r,c}$  is the slope. The steering matrix elements for pass p are defined as:

$$a(\theta_{l,r,c}, v_{l,r,c}, B_{y_c}, B_{z_c}) = e^{-jk(d + r_{l,N})}$$

$$= e^{-jk((v_{l,r,c}t_p - B_{z_c})\cos\theta_{l,r,c} + B_{y_c}\sin\theta_{l,r,c})}, \quad (13)$$

where  $t_p$  is the temporal baseline,  $d = -B_{z_c,p} \cos \theta_{l,r,c} + B_{y_c,p} \sin \theta_{l,r,c}$  is the displacement derived from (11), and  $r_{l,N}$  is the range displacement. The steering vector above is obtained by taking into account the contributions from the layer motion and offsets added to all the monitor pass sensors because of the GPS error.

We can rewrite the joint estimation log-likelihood function as:

$$L(\theta, v, B_z, B_y) = \sum_{c=1}^{N_x} \sum_{r=1}^{N_t} L_{r,c},$$
(14)

where  $N_x$  is the number of along-track samples in the complex SAR image (i.e., number of range lines in the azimuth dimension) and  $N_t$  is the number of fast-time samples in the complex SAR image (i.e., number of snapshots in the range dimension) to consider in the joint estimation. As in (8) the joint maximum likelihood estimation is achieved by doing the maximization across all these log likelihood cost functions:

$$\theta, v, B_z, B_y = \arg \max_{\theta, v, B_z, B_y} \sum_{c=1}^{N_x} \sum_{r=1}^{N_t} (P_{A(\theta, v, B_z, B_y)} R).$$
 (16)

# G. Joint estimation simulation

In order to evaluate the performance of our MLE framework under realistic conditions, we generated a set of synthetic radar data sets with various SNR ranging from 1 to 30. These radar data sets include a signal of subsurface glacier change. The surface accumulation in these synthetic experiments was chosen to be 1 ma<sup>-1</sup> with a linear vertical velocity profile that decreased to zero at the glacier bed (i.e., no basal melt). We assume no along-track variability in sliding parameters, focusing only on uncertainty induced by spatial baseline and across-track slope range estimate errors.

Each synthetic radar data set contains 2 passes, each pass containing radar images recorded from 15 separate antenna

elements. 15 elements were chosen to match the number of elements on the airborne MCoRDS system. Each radar image in each data set contains 100 cross-track pixels and 50 along-track pixels.

The vertical velocities were used to generate 15 independent monitor images, assuming a single value for the cross-track slope, absolute slope, and absolute baseline error. The values for cross-track slope and absolute slope were selected from uniform distributions between -1 and 1 degrees, while the baseline error was selected from a uniform distribution between 0 and 0.1 m.

The joint MLE framework outlined above was run for each monitor-baseline image pair. The interior point method was used to calculate a search direction for the MLE parameters throughout the optimization. The optimum likelihood functions were then summed across all antenna element pairs. The joint estimate for the vertical velocity, cross-track slope, and baseline errors is the set of parameters that gives the highest summed likelihood across all antenna elements. These estimates can then be compared with known values used to derive the synthetic data, and used to evaluate MLE performance.

# III. RESULTS AND DISCUSSION

# A. Joint estimation simulation results

Results for the synthetic simulation described in the previous section are shown in Figures 5-7. Across all simulations, the root-mean-square-error (RMSE) determined by comparing the joint estimated parameters with their ground truth values was reduced as the signal-to-noise ratio (SNR) increased.

The MLE framework we have implemented provides a formal measure of the system errors and solutions for vertical ice-velocity. The flexibility of the adopted MLE framework makes it easy to include additional prior information that constrains the flow behavior and geometry of the layer slopes and vertical deformation. It also can be used to determine the covariance matrix that describes the degeneracy of errors and solutions for vertical deformation. This is an important first step toward evaluating the significance of higher-order terms in non-linear models of vertical deformation.

The MLE framework allows us to incorporate additional observational constraints in the estimation of subsurface properties. This work could be expanded to include the surface horizontal velocity and snow accumulation rate as additional constraints on the inversion. The vertical velocity is equal to the surface accumulation when the ice sheet is in steady state and this may be estimated from other remote sensing measurements, firn core data or weather models [8]. Similarly, the horizontal velocity can be measured from satellite remote sensing measurements [9] and used with analytic descriptions of vertical velocity [10],or three-dimensional thermomechanically coupled models of ice flow [11].

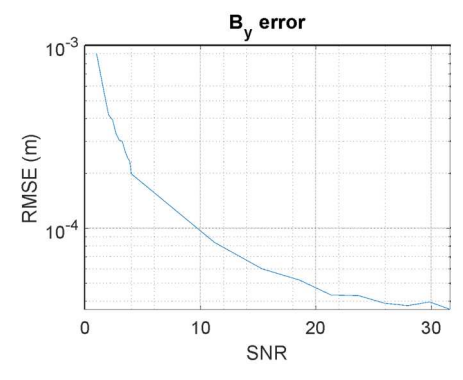


Fig. 5. RMSE plot for baseline errors

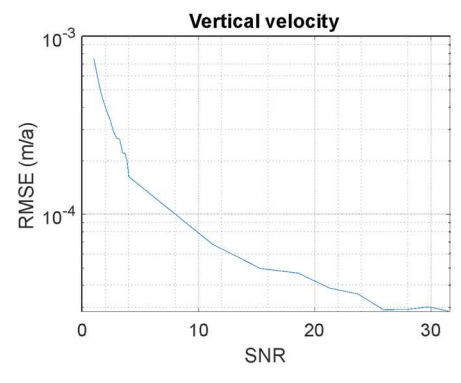


Fig. 6. RMSE plot for vertical velocity

#### IV. CONCLUSION

We have developed an MLE framework that can be used to jointly estimate the baseline and slope errors in addition to the solutions for the ice vertical velocity. This framework reduces the dependence of a solution on the assumptions of a single correction and the ordering of applied corrections through the traditional DInSAR processing workflow.

Where repeat acquisitions exist in the NASA Operation IceBridge (OIB) radar data archive, we intend to apply the MLE framework for interferometric processing. This will result in the concurrent production of fine-resolution maps of the subglacial topography and direct observations of ice deformation and transport from measured englacial vertical velocities. These data products will be used to evaluate ice flow on various timescales, which will expand our understanding of glacier processes that affect ice discharge to the ocean and subsequently sea-level rise.

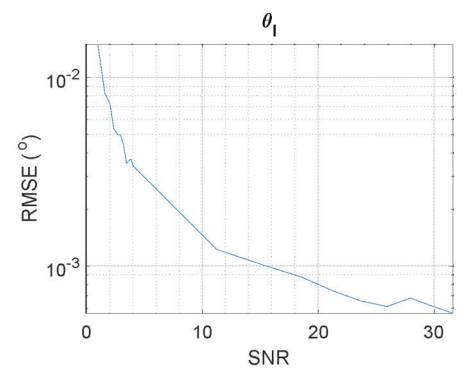


Fig. 7. RMSE plot for slope

# ACKNOWLEDGMENT

We acknowledge the use of data from CReSIS generated with support from NASA 80NSSC21K0753, NASA NNX16AH54G, NSF ACI-1443054, OPP-1739003, and IIS-1838230, Lilly Endowment Incorporated, and Indiana METACyt Initiative.

# REFERENCES

- J. Mouginot, E. Rignot, B. Scheuchl. Continent-Wide, Interferometric SAR Phase, Mapping of Antarctic Ice Velocity. Geophysical Research Letters, American Geophysical Union, 2019, 46 (16), pp.9710-9718. ff10.1029/2019GL083826ff. ffhal-02392132
- P. A. Rosen *et al.*, "Synthetic aperture radar interferometry," in *Proceedings of the IEEE*, vol. 88, no. 3, pp. 333-382, March 2000, doi: 10.1109/5.838084.
- Ziskind, Ilan & Wax, Mati. (1988). Maximum Likelihood Localization of Multiple Sources by Alternating Projection. Acoustics, Speech and Signal Processing, IEEE Transactions on. 36. 1553 1560. 10.1109/29.7543.
- M. A. Doron, A. J. Weiss and H. Messer, "Maximum-Likelihood Direction Finding of Wide-Band Sources," in IEEE Transactions on Signal Processing, vol. 41, no. 1, pp. 411-, January 1993, doi: 10.1109/TSP.1993.193166.
- [5] B. Miller, G. Ariho, J. Paden and E. Arnold, "Multipass SAR Processing for Radar Depth Sounder Clutter Suppression, Tomographic Processing, and Displacement Measurements," IGARSS 2020 2020 IEEE International Geoscience and Remote Sensing Symposium, 2020, pp. 822-825, doi: 10.1109/IGARSS39084.2020.9324498.
- F. Rodriguez-Morales et al., "Advanced Multifrequency Radar Instrumentation for Polar Research," in IEEE Transactions on Geoscience and Remote Sensing, vol. 52, no. 5, pp. 2824-2842, May 2014, doi: 10.1109/TGRS.2013.2266415.
- J. Paden, T. Akins, D. Dunson, C. Allen, and P. Gogineni, "Ice-sheet bed 3-D tomography," Journal of Glaciology, vol. 56, no. 195, pp. 3–11, 2010.
- 3-D tomography," Journal of Glaciology, vol. 56, no. 195, pp. 3–11, 2010. Koenig, L., et al., Annual Greenland accumulation rates (2009–2012) from airborne snow radar. The Cryosphere, 2016. 10: p. 1739-1752. Joughin, I., R. Kwok, and M. Falnestock, Estimation of ice-sheet motion using satellite radar interferometry: method and error analysis with application to Humboldt Glacier, Greenland. Journal of Glaciology, 1996. 42: p. 564-575.
  Theresa Moore, John Paden, Array Manifold Calibration for Multichannel Radar Ice Sounders, in IGARSS 2020, 2020. p. 92-95. Kingslake, J., et al., Full-depth englacial vertical ice-sheet velocities measured using phase-sensitive radar. Journal of Geophysical Research: Earth Surface, 2014. 119. 2604–2618, doi:10.1002/2014JF003275.